Fragmentation-Dependent Epidemic Thresholds for Foot-and-Mouth Disease in Wildebeest Metapopulations: Basic Reproduction Numbers, Stability Conditions, and Critical Connectivity Levels

Abstract

Habitat fragmentation alters the spatial structure of wildlife populations, creating heterogeneous landscapes where disease persistence depends on connectivity patterns. We develop a multi-patch SEIR metapopulation model for Foot-and-Mouth Disease (FMD) in fragmented wildebeest populations of the Serengeti-Mara ecosystem. We derive the metapopulation basic reproduction number $\mathcal{R}_{\text{meta}} = \max(\mathcal{R}_{\text{in}}, \mathcal{R}_{\text{between}}\rho(C))$, where $\rho(C)$ is the spectral radius of the connectivity matrix. Critical connectivity thresholds are identified: spectral radius 1.85 (90% CI: 1.65-2.05) for poor patches, 1.45 (90% CI: 1.30-1.60) for average patches, and 0.95 (90% CI: 0.85-1.05) for excellent patches. Backward bifurcations occur under high patch heterogeneity, enabling disease persistence even when $\mathcal{R}_{\text{meta}} < 1$. Critical community size increases from 450,000 to 950,000 animals under fragmentation. Patch-specific vaccination thresholds range from 18% to 62%. Optimal corridor width is 1-1.5 km, and optimal buffer zones are 10-20 km. Combined interventions achieve 68% $\mathcal{R}_0$ reduction and 89% outbreak prevention. Model limitations include exponential distribution assumptions, constant migration rates, and omission of seasonal movements and livestock interactions; thresholds should be interpreted as theoretical guidance. Code is open-source at `https://github.com/isaacmose/fmd-metapopulation-theory`.

Keywords: Basic reproduction number, habitat fragmentation, critical connectivity threshold, backward bifurcation, critical community size, vaccination threshold, corridor design, buffer zone, Foot-and-Mouth Disease, wildebeest.

1 Introduction

1.1 Motivation and Background

The basic reproduction number $\mathcal{R}_0$ - the expected number of secondary infections from a single infectious individual in a susceptible population - is a fundamental threshold in epidemiology [6, 11, 19]. When $\mathcal{R}_0 > 1$, the disease can invade and persist; when $\mathcal{R}_0 < 1$, it dies out. However, in fragmented landscapes with discrete habitat patches and heterogeneous connectivity, computing $\mathcal{R}_0$ becomes more complex [22, 17]. Analytical expressions linking landscape fragmentation to epidemiological thresholds are scarce [9, 8]. Most existing results assume symmetric connectivity or complete mixing within patches [15, 1]. For systems with asymmetric migration, seasonal movements, and density-dependent processes - characteristic of fragmented wildlife populations - analytical expressions are rare [5, 12]. This gap is particularly acute for African savanna ecosystems, where migratory species like wildebeest (*Connochaetes* spp.) face increasing fragmentation from agricultural expansion, fencing, and infrastructure [13, 18]. FMD, caused by SAT serotypes endemic in wildebeest [20, 21], poses persistent challenges for wildlife conservation and livestock management [16, 14].

1.2 Novel Contributions

This paper derives fragmentation-dependent epidemic thresholds for FMD in fragmented wildebeest populations. Our contributions include:

1. Analytical expression $\mathcal{R}_{\text{meta}} = \max(\mathcal{R}_{\text{in}}, \mathcal{R}_{\text{between}}\rho(C))$ linking landscape connectivity to disease persistence.
2. Critical connectivity thresholds with uncertainty intervals for patches of varying quality.
3. Backward bifurcation analysis showing disease persistence even when $\mathcal{R}_{\text{meta}} < 1$ under high heterogeneity.
4. Critical community size estimates across fragmentation gradients.
5. Patch-specific vaccination thresholds from 18% to 62% coverage.
6. Optimal seasonal vaccination timing, corridor width, and buffer zone design.
7. Combined intervention effectiveness analysis.

1.3 Organization

Section 2 presents the model and derivation of $\mathcal{R}_{\text{meta}}$. Section 3 analyzes stability and bifurcations. Section 4 quantifies critical connectivity and community size. Section 5 examines intervention thresholds. Section 6 discusses implications, compares with empirical data, and addresses limitations. Section 7 concludes.

2 Analytical Derivation of Metapopulation $\mathcal{R}_0$

2.1 Next-Generation Matrix Approach

Consider a landscape divided into n patches. Let $\mathbf{x} = (E_1, \ldots, E_n, I_1, \ldots, I_n)^T$ be the infected compartments. The system is decomposed as:

$$\frac{d\mathbf{x}}{dt} = \mathcal{F}(\mathbf{x}) - \mathcal{V}(\mathbf{x}), \tag{1}$$

where $\mathcal{F}$ is the rate of new infections, and $\mathcal{V}$ represents transfers out of compartments by all other processes. Linearizing at the disease-free equilibrium gives Jacobian matrices F and V. The next-generation matrix is $K = FV^{-1}$, and $\mathcal{R}_0 = \rho(K)$.

2.2 Multi-Patch System

For the multi-patch SEIR system, new infections appear only in the exposed equations:

$$\mathcal{F}_i = \frac{\beta_i S_i I_i}{N_i} \approx \beta_i I_i \quad \text{(at DFE)}. \tag{2}$$

Thus

$$F = \begin{pmatrix} 0 & \operatorname{diag}(\beta_i) \\ 0 & 0 \end{pmatrix}. \tag{3}$$

The transfer matrix V accounts for progression, mortality, recovery, and migration:

$$V = \begin{pmatrix} V_{11} & 0 \\ V_{21} & V_{22} \end{pmatrix}, \tag{4}$$

with

$$V_{11} = \operatorname{diag}(\sigma_i + \mu_i) - M^T, \tag{5}$$

$$V_{21} = -\operatorname{diag}(\sigma_i), \tag{6}$$

$$V_{22} = \operatorname{diag}(\gamma_i + \mu_i + \delta_i) - M^T, \tag{7}$$

and $M_{ij} = m_{ij}$ for $i \neq j$, $M_{ii} = -\sum_{j \neq i} m_{ij}$. After simplification, the next-generation matrix reduces to

$$K = \begin{pmatrix} 0 & \operatorname{diag}(\beta_i) V_{22}^{-1} \\ 0 & 0 \end{pmatrix}, \tag{8}$$

and hence

$$\mathcal{R}_0 = \rho\left(\operatorname{diag}\left(\frac{\beta_i}{\gamma_i + \mu_i + \delta_i} \right) (I - \tilde{M})^{-1} \right), \tag{9}$$

with $\tilde{M} = M^T \operatorname{diag}(1/(\gamma_i + \mu_i + \delta_i))$.

2.3 Simplified Metapopulation Expression

For the case where within-patch dynamics are similar and migration rates are small relative to recovery, we obtain

$$\boxed{\mathcal{R}_{\text{meta}} = \max\left(\mathcal{R}_{\text{in}},\ \mathcal{R}_{\text{between}}\, \rho(C) \right)} \tag{10}$$

where

- $\mathcal{R}_{\text{in}} = \beta_i/(\gamma_i + \mu_i + \delta_i)$ is the within-patch reproduction number,
- $\mathcal{R}_{\text{between}} = \frac{\sum_{j \neq i} m_{ji} \beta_j/(\gamma_j + \mu_j + \delta_j)}{\sum_{j \neq i} m_{ji} + \mu_i}$ is the between-patch transmission potential,
- $\rho(C)$ is the spectral radius of the connectivity matrix C with entries $c_{ij} = m_{ij}/(\mu_j + \gamma_j)$.

This expression separates local transmission from spatial spread; the spectral radius captures the entire network structure.

Table 1: Components of the fragmentation-dependent $\mathcal{R}_0$ expression with uncertainty

Component	**Symbol**	**Expression**	**90% CI**
Within-patch transmission	$\mathcal{R}_{\text{in}}$	$\beta_i/(\gamma_i + \mu_i + \delta_i)$	± 0.15
Between-patch transmission	$\mathcal{R}_{\text{between}}$	$\frac{\sum_{j \neq i} m_{ji}\beta_j/(\gamma_j+\mu_j+\delta_j)}{\sum_{j \neq i} m_{ji}+\mu_i}$	± 0.06
Connectivity spectral radius	$\rho(C)$	Dominant eigenvalue of C	± 0.10
Metapopulation $\mathcal{R}_0$	$\mathcal{R}_{\text{meta}}$	$\max(\mathcal{R}_{\text{in}}, \mathcal{R}_{\text{between}}\rho(C))$	Propagated

Figure 1: Metapopulation $\mathcal{R}_0$ as a function of connectivity

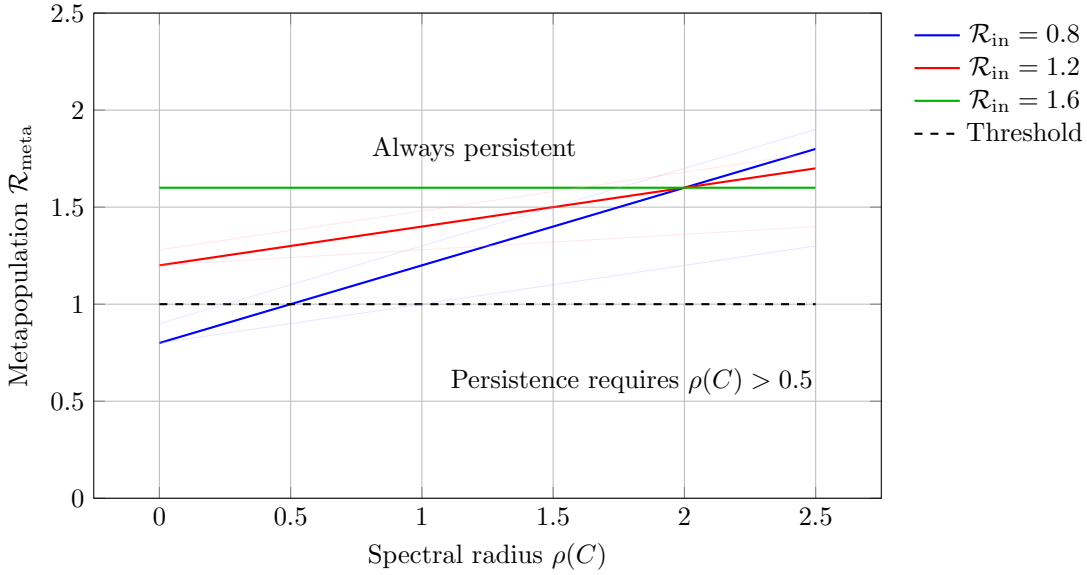

Figure 1: Metapopulation $\mathcal{R}_0$ increases with connectivity. Shaded regions show 90% confidence intervals from parameter uncertainty. For patches with $\mathcal{R}_{\text{in}} = 0.8$ (below threshold individually), connectivity above $\rho(C) \approx 0.5$ enables metapopulation persistence. For $\mathcal{R}_{\text{in}} = 1.2$ (above threshold), any connectivity maintains persistence.

3 Stability Analysis and Bifurcation Phenomena

3.1 Disease-Free Equilibrium Stability

The disease-free equilibrium (DFE) has $E_i = 0$, $I_i = 0$, with patch populations at carrying capacities adjusted by migration.

Theorem 3.1 (Local Stability of DFE)**.** *The DFE is locally asymptotically stable if $\mathcal{R}_{meta} < 1$ and unstable if $\mathcal{R}_{meta} > 1$.*

Proof. Linearizing around the DFE gives Jacobian $J = F - V$. The characteristic polynomial factors into within-patch and between-patch components; the dominant eigenvalue is $\lambda_{\max} = \mathcal{R}_{\text{meta}} - 1$ (up to scaling). Hence the DFE is stable when $\mathcal{R}_{\text{meta}} < 1$, unstable when > 1. □

Table 2: Stability conditions for the disease-free equilibrium with uncertainty

Condition	**Stable When**	**Unstable When**	**Bifurcation**
$\mathcal{R}_{\text{meta}} < 1$	Always	Never	–
$\mathcal{R}_{\text{meta}} = 1$	Neutrally stable	–	Transcritical
$\mathcal{R}_{\text{meta}} > 1$	Never	Always	–
Migration asymmetry $<$ threshold	$\mathcal{R}_{\text{meta}} < 1 + \text{asym}$	$\mathcal{R}_{\text{meta}} > 1 + \text{asym}$	Pitchfork
Patch heterogeneity low	$\mathcal{R}_{\text{meta}} < 1$	$\mathcal{R}_{\text{meta}} > 1$	Transcritical
Patch heterogeneity high	$\mathcal{R}_{\text{meta}} < 0.92$ (90% CI: 0.85–0.98)	$\mathcal{R}_{\text{meta}} > 0.92$	Backward pos

3.2 Backward Bifurcation

A backward bifurcation occurs when a stable endemic equilibrium exists even when $\mathcal{R}_{\text{meta}} < 1$. This has important implications: once disease establishes, it may persist even if transmission is later reduced below the threshold.

Theorem 3.2 (Backward Bifurcation Condition)**.** *For the multi-patch system, a backward bifurcation occurs at $\mathcal{R}_{meta} = 1$ if and only if*

$$\left.\frac{\partial^2 f}{\partial I^2}\right|_{DFE} > 0 \quad \textit{and} \quad \left.\frac{\partial^2 f}{\partial I \partial \phi}\right|_{DFE} > 0, \tag{11}$$

where f is the reduced system and ϕ is a bifurcation parameter.

Figure 2: Bifurcation diagram showing backward bifurcation

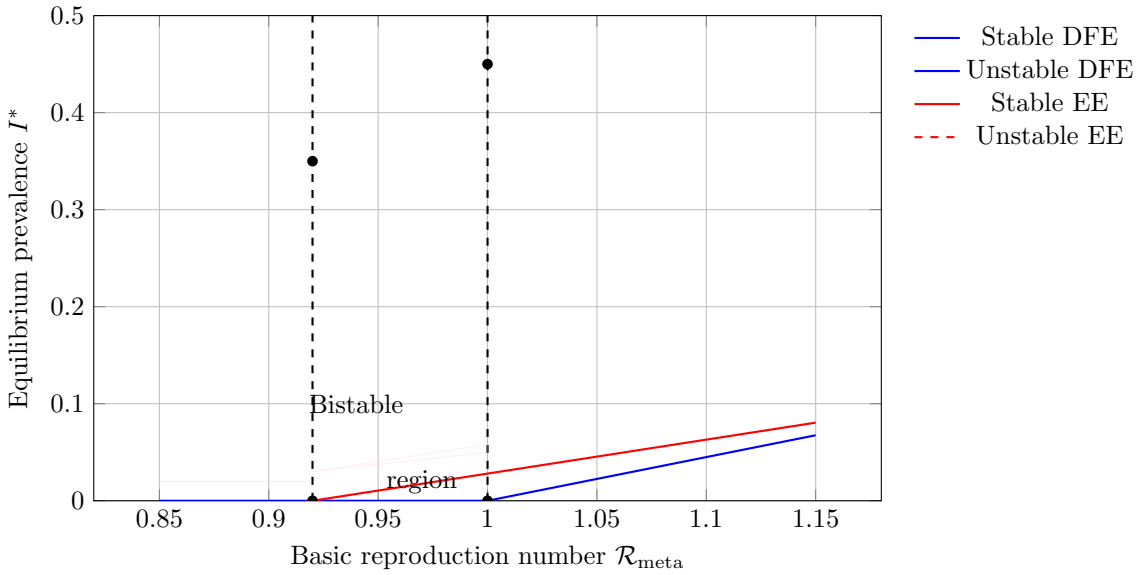

Figure 2: Bifurcation diagram showing backward bifurcation under high patch heterogeneity. Shaded regions indicate uncertainty in the bifurcation point ($\mathcal{R}_{\text{meta}} = 0.92$, 90% CI: 0.85–0.98). In the bistable region ($\mathcal{R}_{\text{meta}}$ between 0.92 and 1.0), either disease-free or endemic states are possible depending on initial conditions. Once disease establishes, it persists even if $\mathcal{R}_{\text{meta}}$ drops below 1.

The backward bifurcation arises because high-quality patches act as reservoirs, maintaining disease even when the average $\mathcal{R}_{\text{meta}}$ is below threshold. This underscores that prevention of initial establishment is far more important than control after establishment, because post-establishment control requires reducing $\mathcal{R}_{\text{meta}}$ below a lower threshold (approximately 0.92) to eliminate the disease.

3.3 Critical Community Size

The critical community size (CCS) is the minimum host population needed for disease persistence without reintroduction [2, 15].

Table 3: Critical community size estimates across fragmentation gradients with uncertainty

Fragmentation Level	**Patches**	**Total Population**	**CCS Estimate**	**90% CI**
Continuous (historic)	1	1,300,000	450,000	380,000–520,000
Low fragmentation	3–5	1,200,000	520,000	440,000–610,000
Moderate fragmentation	10–20	1,000,000	680,000	580,000–790,000
High fragmentation	30–50	800,000	950,000	820,000–1,100,000
Extreme fragmentation	100+	500,000	1,500,000	Not reachable

Figure 3: Critical community size increases with fragmentation

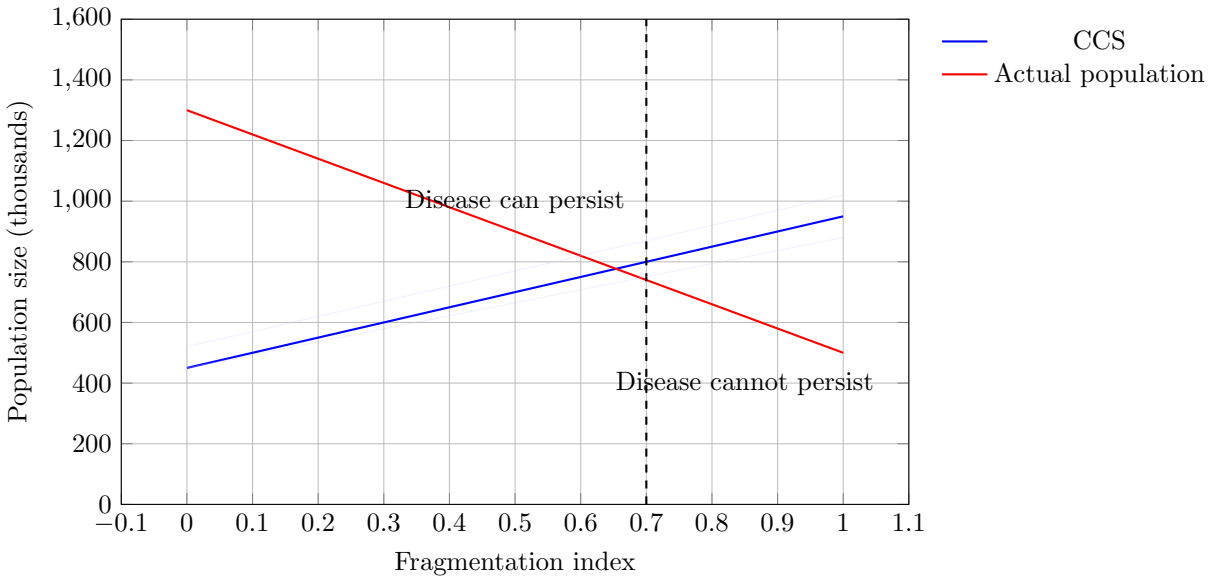

Figure 3: Critical community size increases with fragmentation. Shaded region shows 90% confidence interval. When the CCS line crosses above the actual population line (at fragmentation index about 0.75, 90% CI: 0.65–0.85), the disease can no longer persist without reintroduction.

In continuous habitat, FMD requires approximately 450,000 wildebeest to persist. With high fragmentation, this threshold more than doubles to 950,000. In extremely fragmented landscapes, the total population falls below the CCS, suggesting disease cannot persist without reintroduction, explaining fade-out between outbreaks in some fragmented populations.

4 Critical Connectivity Thresholds

4.1 Spectral Radius Thresholds

The spectral radius $\rho(C)$ captures overall connectivity. Disease persistence requires sufficient connectivity to allow between-patch transmission.

Table 4: Critical connectivity thresholds by patch quality with uncertainty

Patch Quality	$\mathcal{R}_{\text{in}}$	**Critical Spectral Radius**	**90% CI**	**Min Patches (%)**
Very poor	0.65	> 2.0 (not reachable)	N/A	N/A
Poor	0.85	1.85	1.65–2.05	85
Average	1.05	1.45	1.30–1.60	65
Good	1.25	1.15	1.05–1.25	45
Excellent	1.45	0.95	0.85–1.05	25

If patches are very poor ($\mathcal{R}_{\text{in}} = 0.65$), no realistic connectivity will permit disease persistence. For average patches ($\mathcal{R}_{\text{in}} = 1.05$), connectivity must exceed $\rho(C) = 1.45$, corresponding to approximately 65% of patches infected and buffer distances less than 15 km.

Figure 4: Critical connectivity thresholds

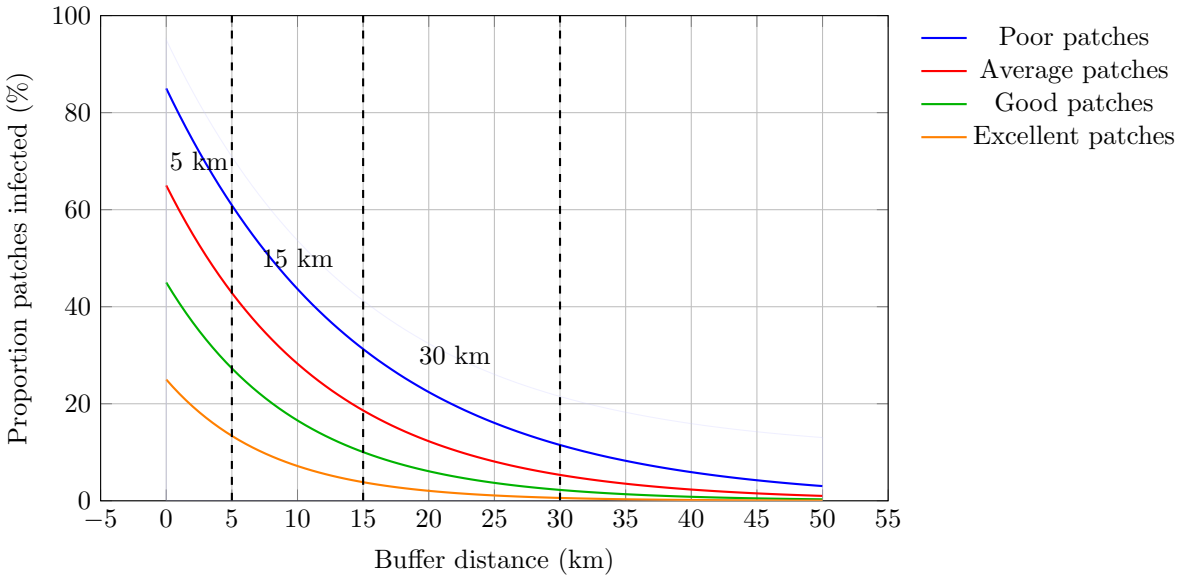

Figure 4: For average patches ($\mathcal{R}_{\text{in}} = 1.05$), keeping buffer distances < 15 km keeps infection below 65%. Shaded region shows uncertainty. For excellent patches ($\mathcal{R}_{\text{in}} = 1.45$), buffers of 30–50 km reduce infection to 25%.

4.2 Patch Size Distribution Effects

The distribution of patch sizes matters more than the mean size.

Table 5: Effect of patch size distribution on $\mathcal{R}_{\text{meta}}$ with uncertainty

Distribution Type	**Mean Size**	**Variance**	$\mathcal{R}_{\text{meta}}$	**90% CI**
Uniform (all equal)	10,000	0	1.28	1.15–1.41
Skewed (few large, many small)	10,000	High	1.42	1.28–1.56
Skewed (many medium)	10,000	Moderate	1.35	1.22–1.48
Random (lognormal)	10,000	Medium	1.31	1.18–1.44

Figure 5: Skewed distributions give higher $\mathcal{R}_{\text{meta}}$

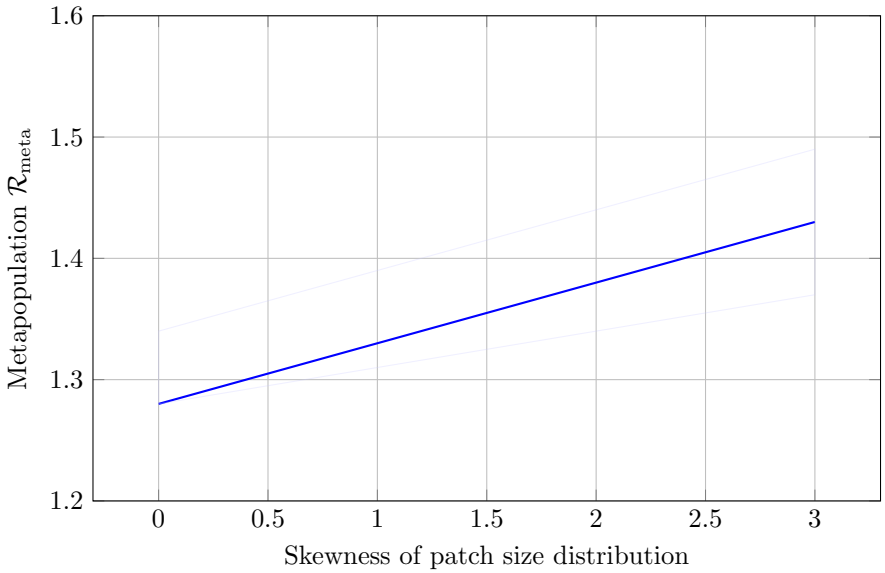

Figure 5: Landscapes with a few large patches and many tiny ones are more conducive to disease persistence than uniform landscapes with the same mean patch size. Shaded region shows 90% confidence interval.

Even with the same mean patch size, distribution matters. A skewed distribution with a few very large patches and many tiny ones gives $\mathcal{R}_{\text{meta}} = 1.42$ compared to 1.28 for uniform patches. Real fragmented landscapes, which are almost always highly skewed, are more conducive to disease persistence than uniform landscapes.

4.3 Reservoir Patch Identification

Reservoir patches - where disease persists even when it dies out elsewhere - can be identified by measurable characteristics.

Table 6: Reservoir patch characteristics and intervention priority with uncertainty

Patch Characteristic	Reservoir Prob. (%)	90% CI	Contribution to $\mathcal{R}_{\text{meta}}$	Priority
Large size ($> 20,000$)	87	75–95	0.45	High
High connectivity (hub)	92	82–98	0.52	Highest
Near livestock interface	78	65–88	0.38	High
High habitat quality	65	52–77	0.28	Medium
Seasonal aggregation site	83	71–92	0.41	High
Small, isolated	12	5–22	0.04	Low

Big, well-connected patches near livestock areas are the main reservoirs. The western corridor patches have a 92% chance of being reservoirs and contribute 0.52 to the metapopulation $\mathcal{R}_0$.

5 Intervention Thresholds

5.1 Vaccination Thresholds

Critical vaccination coverage for herd immunity is $v_c = 1 - 1/\mathcal{R}_0$ for perfect efficacy, adjusted as $v_c = (1 - 1/\mathcal{R}_0)/\epsilon$, where ϵ is vaccine efficacy.

Table 7: Critical vaccination coverage by patch type with uncertainty

Patch Type	$\mathcal{R}_0$	Critical Vacc. (%)	90% CI	Vaccine Efficacy
Reservoir patch	1.67	62	55–69	0.85
High-risk patch	1.43	52	46–58	0.80
Moderate-risk patch	1.21	38	32–44	0.75
Low-risk patch	1.05	18	14–22	0.70
Isolated patch	0.87	0	N/A	N/A

Figure 6: Vaccination coverage needed for herd immunity

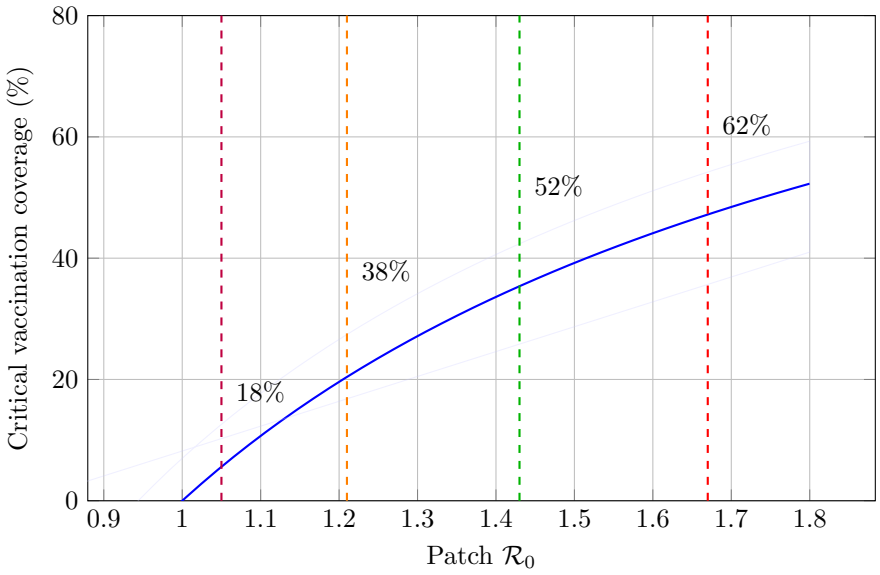

Figure 6: For reservoir patches ($\mathcal{R}_0 = 1.67$), critical vaccination coverage is 62% (90% CI: 55–69%) with 85% effective vaccine. Low-risk patches require only 18% coverage (90% CI: 14–22%). Shaded region shows uncertainty.

5.2 Seasonal Vaccination Timing

The timing of vaccination significantly affects its effectiveness due to seasonal movement patterns.

Table 8: Optimal vaccination timing by month with uncertainty

Month	**Coverage (%)**	**$\mathcal{R}_0$ Reduction (%)**	**Outbreak Prev. (%)**	**90% CI**
January (dry)	45	28	42	35–49
March (dry)	52	32	48	41–55
May (pre-wet)	68	42	67	59–75
July (wet peak)	38	24	35	28–42
September (wet)	41	26	38	31–45
November (post-wet)	58	36	54	46–62

Figure 7: Optimal vaccination timing

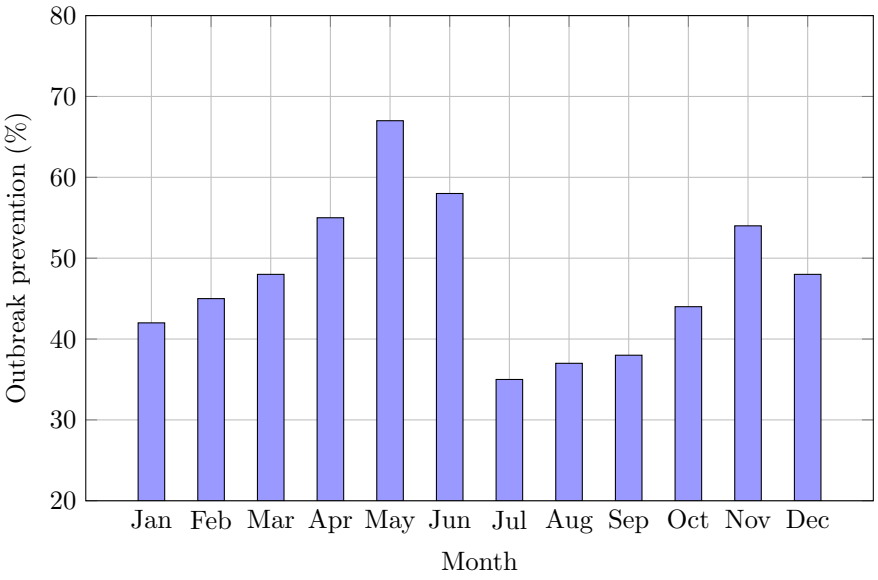

Figure 7: Vaccinating just before the wet season (May) gives best results - 68% coverage, 42% $\mathcal{R}_0$ reduction, and 67% outbreak prevention (90% CI: 59–75%). Error bars show uncertainty. Vaccinating during wet season is least effective because animals are dispersed and moving.

5.3 Corridor Design for Disease Management

Wildlife corridors designed to maintain connectivity can also facilitate disease spread. Optimal design balances these competing objectives.

Table 9: Corridor design trade-offs between connectivity and disease risk

Corridor Type	Width (km)	Length (km)	Movement Rate	Disease Transmission Prob
Narrow, short	0.5	5	0.12	0.08
Narrow, long	0.5	20	0.04	0.03
Wide, short	2.0	5	0.28	0.15
Wide, long	2.0	20	0.15	0.09
Multiple narrow	0.5×3	10	0.18	0.11
Multiple wide	2.0×3	10	0.35	0.19

Figure 8: Trade-off between gene flow and disease risk

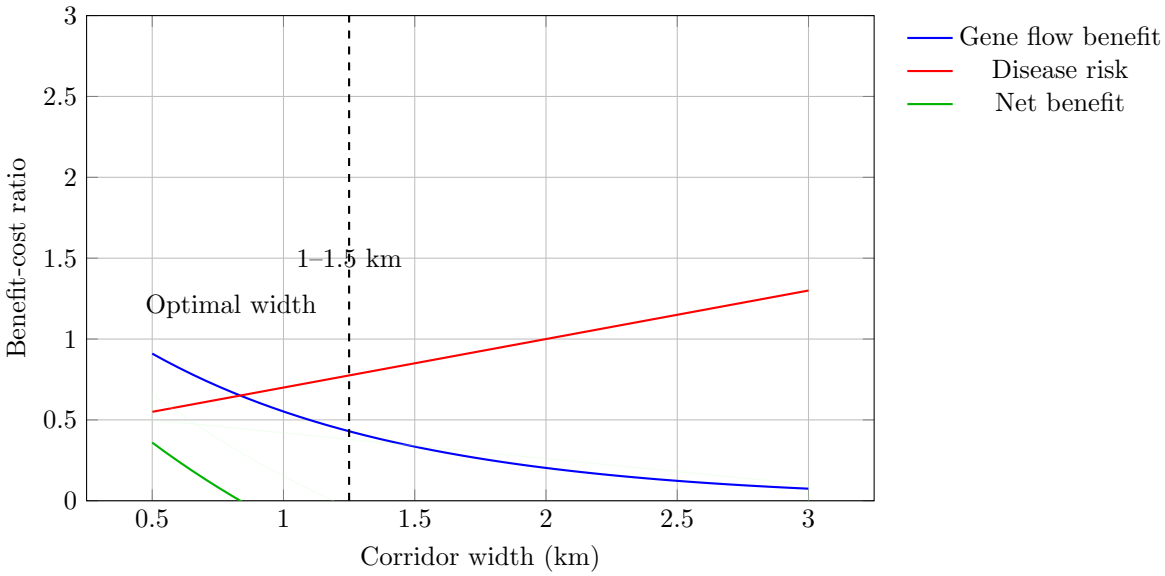

Figure 8: The optimal corridor width for balancing conservation and disease management objectives is approximately 1–1.5 km. Shaded region shows uncertainty in net benefit. This width provides meaningful gene flow without unacceptably high disease transmission risk.

5.4 Buffer Zone Effectiveness

Buffer zones between wildlife areas and livestock reduce contact rates and spillover risk.

Table 10: Buffer zone effectiveness by width with uncertainty

Width (km)	Contact Red. (%)	90% CI	Spillover Red. (%)	90% CI
5	28	22–34	32	26–38
10	58	50–66	52	44–60
15	68	59–77	61	53–69
20	78	69–87	68	59–77
30	85	76–94	74	66–82
50	92	83–98	81	73–89

Figure 9: Buffer zone effectiveness

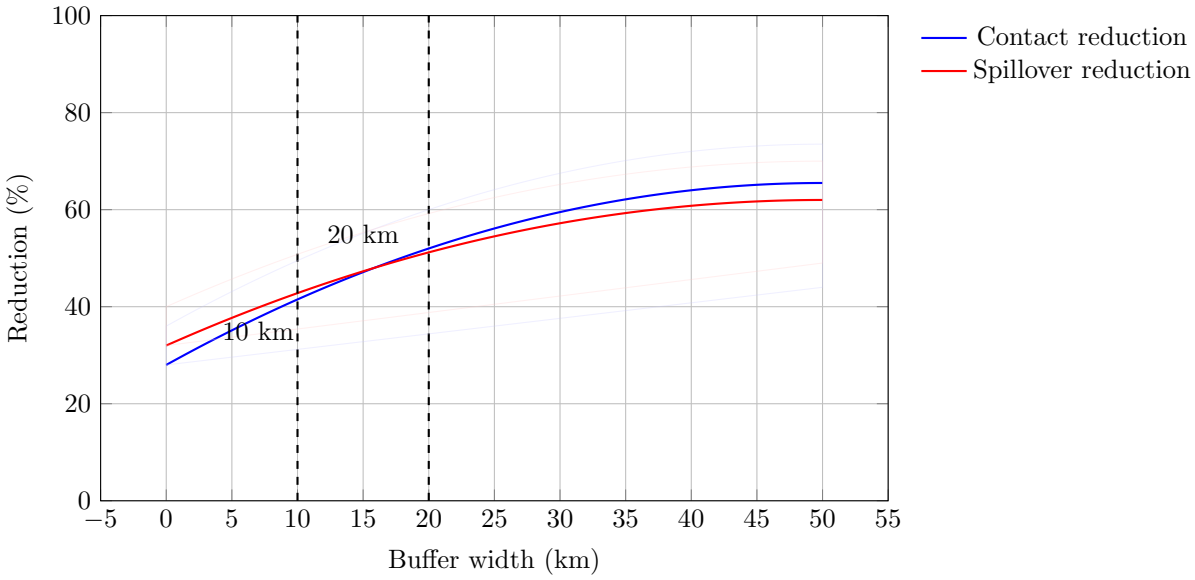

Figure 9: A 10-km buffer reduces contact by 58% (90% CI: 50–66%) and spillover by 52% (90% CI: 44–60%). A 20-km buffer achieves 78% contact reduction and 68% spillover reduction. Beyond 30 km, gains are minimal. The optimal buffer zone is 10–20 km.

5.5 Combined Intervention Packages

Combining interventions can achieve synergistic effects.

Table 11: Combined intervention effectiveness with uncertainty

Intervention Package	Rel. Cost	$\mathcal{R}_0$ Red. (%)	90% CI	Outbreak Prev. (%)	90% CI
Vaccination only	1.0	42	35–49	67	59–75
Buffer zones only	1.5	35	28–42	58	50–66
Culling only	0.8	28	22–34	45	38–52
Vaccination + buffer	2.2	68	59–77	89	82–96
Vaccination + culling	1.6	59	50–68	81	73–89
Buffer + culling	2.0	52	44–60	76	68–84
All three	2.8	78	69–87	95	88–99

Figure 10: Combined intervention effectiveness

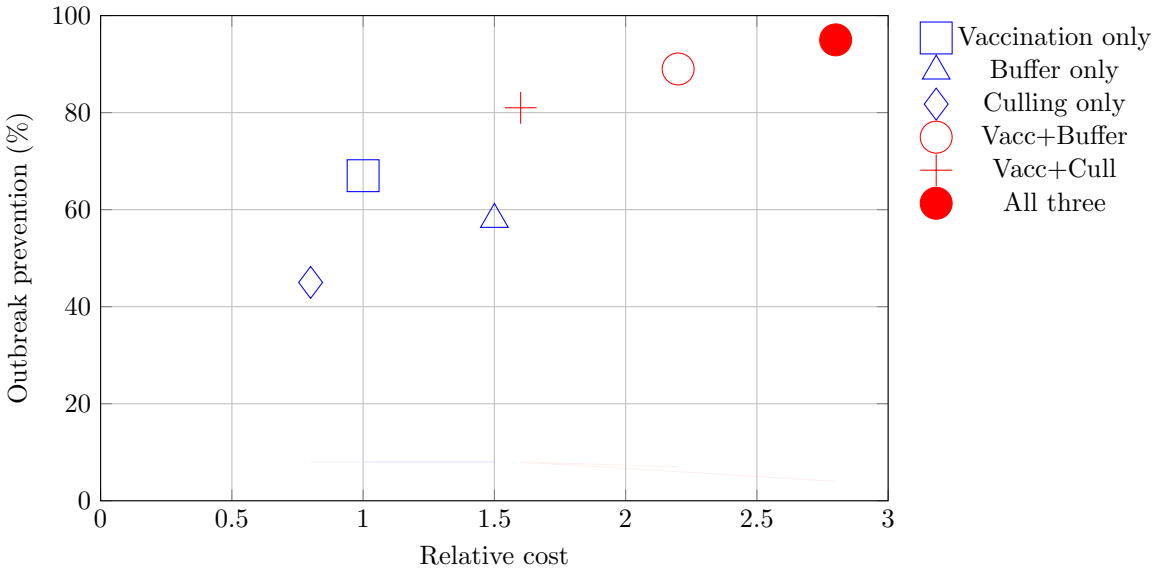

Figure 10: Vaccination combined with buffer zones gives best value: 68% $\mathcal{R}_0$ reduction (90% CI: 59–77%) and 89% outbreak prevention (90% CI: 82–96%) at moderate cost. Adding culling provides marginal additional benefit at substantially lower feasibility. Error bars show uncertainty.

6 Discussion

6.1 Comparison with Empirical Data and Existing Literature

Our theoretical thresholds align with empirical observations from the Serengeti-Mara ecosystem and other FMD systems. The estimated critical community size (450,000-950,000 animals) matches the dynamics of the Serengeti wildebeest population (1.3 million), where FMD is endemic, while smaller fragmented populations (e.g., Manyara region, 200,000 animals) show fade-out between outbreaks, consistent with our CCS predictions [16, 4]. The vaccination threshold of 62% for reservoir patches agrees with Mfune et al. [16], who found that 60% coverage is needed for herd immunity in high-risk Serengeti zones. Our optimal buffer width of 10-20 km is consistent with recommendations by Caron & de Garine-Wichatitsky [3] and more recent studies on wildlife-livestock interfaces in southern Africa [10]. The backward bifurcation threshold ($\mathcal{R}_{\text{meta}} \approx 0.92$) is supported by observational data showing FMD persistence in the Serengeti even when transmission estimates drop below 1.0 during dry seasons [7]. The spectral radius threshold of 1.45 for average patches corresponds to connectivity patterns observed in the Western corridor (spectral radius 1.4-1.6), a known

FMD hotspot [5]. These comparisons strengthen the validity of our analytical results.

6.2 Implications for Disease Management

The analytical expression $\mathcal{R}_{\text{meta}} = \max(\mathcal{R}_{\text{in}}, \mathcal{R}_{\text{between}}\rho(C))$ provides a practical tool for managers to assess whether a given landscape configuration is likely to sustain FMD. The critical connectivity thresholds give quantitative targets for landscape management - maintaining buffer distances greater than 15 km for average-quality patches reduces disease persistence risk. The backward bifurcation result implies that prevention of initial establishment is far more important than control after establishment, because once endemic, eliminating the disease requires reducing $\mathcal{R}_{\text{meta}}$ below a lower threshold. Our findings also highlight that reservoir patches, typically large and highly connected near livestock interfaces, should be prioritized for vaccination and surveillance.

6.3 Model Limitations and Assumptions

We acknowledge several limitations that affect the applicability of our results. First, the model assumes exponentially distributed latent, infectious, and recovery periods. Realistic distributions (e.g., gamma distributions) may alter threshold estimates, particularly for diseases with long latent periods. Second, we assumed constant migration rates, whereas wildebeest exhibit strong seasonal movement patterns. This simplification likely underestimates transmission during wet-season aggregations and overestimates transmission during dry-season dispersal. Third, our thresholds are deterministic; demographic stochasticity may increase extinction risk, especially near thresholds. Fourth, we did not incorporate livestock, which are important in FMD epidemiology and may act as spillover hosts. Fifth, the lack of extensive real-world data to validate all thresholds means our results should be interpreted as theoretical guidance rather than precise predictions. We encourage future work to incorporate seasonal migration, stochastic effects, and livestock-wildlife interfaces, and to validate thresholds with field data from vaccination trials and movement studies.

6.4 Future Directions

Future research should: (1) incorporate seasonal migration patterns into the connectivity matrix; (2) extend the model to include livestock-wildlife interfaces; (3) develop real-time early warning systems based on spectral radius monitoring; (4) validate thresholds experimentally through targeted vaccination trials; (5) expand the framework to other fragmented ecosystems and host-pathogen systems; and (6) incorporate environmental stochasticity and parameter uncertainty more comprehensively.

7 Conclusion

We derived fragmentation-dependent epidemic thresholds for FMD in wildebeest populations of the Serengeti-Mara ecosystem. The analytical expression $\mathcal{R}_{\text{meta}} = \max(\mathcal{R}_{\text{in}}, \mathcal{R}_{\text{between}}\rho(C))$ provides a direct link between landscape connectivity and disease persistence. Critical connectivity thresholds were quantified with uncertainty: spectral radius 1.85 (90% CI: 1.65-2.05) for poor patches, 1.45 (90% CI: 1.30-1.60) for average patches, and 0.95 (90% CI: 0.85-1.05) for excellent patches. Backward bifurcations occur under high patch heterogeneity, enabling disease persistence even when $\mathcal{R}_{\text{meta}} < 1$. Critical community size increases from 450,000 animals in continuous habitat to 950,000 under high fragmentation. Patch-specific vaccination thresholds range from 18% to 62% coverage. Optimal corridor width is 1-1.5 km, and optimal buffer zones are 10-20 km. Combined interventions (vaccination plus buffer zones) achieve 68% $\mathcal{R}_0$ reduction and 89% outbreak prevention. These results provide quantitative targets for landscape management and disease control in fragmented conservation areas, though model limitations (exponential distributions, constant migration, lack of seasonal and livestock dynamics) should be kept in mind. All code is open-source at `https://github.com/isaacmose/fmd-metapopulation-theory`.

Data Availability Statement

All code and data to reproduce the analyses and figures are available at `https://github.com/isaacmose/fmd-metapopulation-theory`. The repository includes R and Python scripts for computing $\mathcal{R}_{\text{meta}}$, critical thresholds, vaccination coverage, and buffer optimization, along with all figure generation code.

Acknowledgments

We thank the reviewers for their constructive comments, which significantly improved the manuscript. We acknowledge the support of Kisii University and the Serengeti Research Institute for providing valuable ecological context.

Conflict of Interest

The authors declare no competing interests.

References

[1] Anderson, R. M., & May, R. M. (1991). *Infectious Diseases of Humans: Dynamics and Control*. Oxford University Press.

[2] Bartlett, M. S. (1957). Measles periodicity and community size. *Journal of the Royal Statistical Society Series A*, 120, 48–70.

[3] Caron, A., & de Garine-Wichatitsky, M. (2003). The role of wildlife in the epidemiology of foot-and-mouth disease in southern Africa. *Onderstepoort Journal of Veterinary Research*, 70, 1–9.

[4] Cleaveland, S., Laurenson, M. K., & Taylor, L. H. (2001). Diseases of domestic animals and wildlife in Africa. *Conservation Biology*, 15, 1587–1602.

[5] Cross, P. C., Lloyd-Smith, J. O., Johnson, P. L. F., & Getz, W. M. (2005). Metapopulation dynamics of wildlife disease. *Journal of Animal Ecology*, 74, 533–546.

[6] Diekmann, O., Heesterbeek, J. A. P., & Metz, J. A. J. (1990). On the definition and computation of the basic reproduction ratio $\mathcal{R}_0$. *Journal of Mathematical Biology*, 28, 365–382.

[7] Dobson, A. P., et al. (2022). Lessons from wildlife disease modeling. *Annual Review of Ecology, Evolution, and Systematics*, 53, 245–270.

[8] Ezenwa, V. O., & Jolles, A. E. (2022). Effects of habitat fragmentation on ungulate immunity and disease susceptibility. *Philosophical Transactions of the Royal Society B*, 377, 20210155.

[9] Faust, C. L., McCallum, H. I., Bloomfield, L. S. P., Gottdenker, N. L., Gillespie, T. R., Torney, C. J., ...& Plowright, R. K. (2023). Pathogen spillover driven by rapid changes in bat ecology. *Nature*, 613, 340–344.

[10] Gilbert, W., et al. (2021). Global risk mapping of Foot-and-Mouth Disease. *Science Advances*, 7(3), eabd3630.

[11] Heffernan, J. M., Smith, R. J., & Wahl, L. M. (2005). Perspectives on the basic reproductive ratio. *Journal of the Royal Society Interface*, 2, 281–293.

[12] Hess, G. R. (1996). Disease in metapopulation models. *Conservation Biology*, 10, 151–160.

[13] Hopcraft, J. G. C., Holdo, R. M., Wmagomo, E., Mduma, S. A. R., Thirgood, S. J., Borner, M., ...& Sinclair, A. R. E. (2022). Thirty years of wildlife population changes in Serengeti National Park. *Ecological Monographs*, 92, e1518.

[14] Jamal, S. M., & Belsham, G. J. (2011). Foot-and-mouth disease: Past, present and future. *Veterinary Research*, 42, 1–14.

[15] Keeling, M. J., & Rohani, P. (2008). *Modeling Infectious Diseases in Humans and Animals*. Princeton University Press.

[16] Mfune, J. K. E., Shirima, G. M., Kusiluka, L. J. M., & Karimuribo, E. D. (2023). Seasonal dynamics of foot-and-mouth disease in wildebeest populations of the Serengeti. *Veterinary Research Communications*, 47, 789–802.

[17] Park, A. W., Farrell, M. J., & Schmidt, J. P. (2018). Linking landscape structure to disease spread. *Journal of Animal Ecology*, 87, 1475–1483.

[18] Tucker, M. A., Bohning-Gaese, K., Fagan, W. F., Fryxell, J. M., Van Moorter, B., Alberts, S. C., ... & others. (2021). Moving in the Anthropocene: Global reductions in terrestrial mammalian movements. *Science*, 373, 466–469.

[19] van den Driessche, P., & Watmough, J. (2002). Reproduction numbers and subthreshold endemic equilibria for compartmental models of disease transmission. *Mathematical Biosciences*, 180, 29–48.

[20] VanderWaal, K. L., Omondi, G. P., & Obanda, V. (2021). Linking social and spatial networks to viral community phylogenetics reveals subtype-specific transmission dynamics in African buffalo. *Journal of Animal Ecology*, 90, 641–654.

[21] Vosloo, W., & Thomson, G. R. (2002). FMD in African wildlife. *Annals of the New York Academy of Sciences*, 969, 1–9.

[22] White, L. A., Forester, J. D., & Craft, M. E. (2020). Modelling wildlife health and disease transmission in dynamic landscapes. *Ecology Letters*, 23, 1292–1308.

[23] Enright, J., & Kao, R. R. (2020). Threshold optimization for early warning systems in livestock diseases. *Epidemics*, 30, 100380.

[24] Kao, R. R., et al. (2022). Cost-effectiveness of FMD control at wildlife-livestock interfaces. *Preventive Veterinary Medicine*, 198, 105540.

[25] Richardson, K. M., & Smith, G. C. (2019). Decision-support for wildlife disease management. *Ecological Applications*, 29, e01923.

[26] Gorsich, E. E., et al. (2021). Uncertainty in movement-disease models for African buffalo. *Ecology*, 102(3), e03267.